

<https://doi.org/10.1038/s41535-026-00900-9>

# Altermagnetism and weak ferromagnetism

Igor Solovyev<sup>1</sup>✉, Sergey Nikolaev<sup>2</sup> & Akihiro Tanaka<sup>1</sup>

Using a realistic model relevant to  $\text{La}_2\text{CuO}_4$  and other altermagnetic perovskites, we study interrelations between weak spin ferromagnetism, anomalous Hall conductivity,  $\sigma_{xy}$ , and net orbital magnetization  $\mathcal{M}$ . All of them are intertwined with the vector of Dzyaloshinskii-Moriya interactions. Nevertheless, while weak spin ferromagnetism is induced by interactions having the same sign in all equivalent bonds,  $\sigma_{xy}$  and  $\mathcal{M}$  are related to sign-alternating interactions, which do not contribute to any canting of spins. The microscopic model remains invariant under the symmetry operation  $\{S|\mathbf{t}\}$ , combining the shift  $\mathbf{t}$  of antiferromagnetically coupled sublattices to each other with the spin flip  $S$ . Thus, the band structure remains spin-degenerate, but the time-reversal symmetry is broken, providing a possibility to realize  $\sigma_{xy}$  in antiferromagnetic substances. The altermagnetic splitting of bands, breaking  $\{S|\mathbf{t}\}$ , does not play a major role in the problem. More important is the orthorhombic strain, responsible for finite  $\sigma_{xy}$  and  $\mathcal{M}$ .

**Preface** Daniel Khomskii had a unique ability of finding the logic behind seemingly complicated phenomena and internal connections between their different facets. He substantially enriched the conventional theory of magnetism by decorating it with intertwined orbital, lattice, and other degrees of freedom. While basically an observer in the field of electronic structure calculations, he made enormous contributions to it by providing a rational explanation for many puzzles and finding simplified toy models capturing the essence of complex computer simulations. This article, which illustrates the potential of the toy model analysis and explains the deep intertwining between new and old concepts of unconventional antiferromagnetism, known as, respectively, altermagnetism and weak ferromagnetism, is a tribute to his memory.

Altermagnetism is regarded as a new phase of matter, where a nearly antiferromagnetic (AFM) alignment of spins coexists with the spin splitting of bands and robust time-reversal symmetry ( $\mathcal{T}$ ) breaking, which are typical for ferromagnetic (FM) systems<sup>1–4</sup>. Nevertheless, this new classification raises new questions, especially on how it fits into our previous knowledge on AFM materials. It is certainly true that the lifting of Kramers' degeneracy of AFM bands, which was predicted largely due to development of density-functional theory (DFT) calculations, is a new aspect of the problem<sup>5–12</sup>. On the other hand, the possibility of breaking  $\mathcal{T}$  in certain classes of AFM systems has been known for decades. As was pointed out by Dzyaloshinskii<sup>13</sup>, using phenomenological symmetry arguments, the materials whose magnetic unit cell coincides with the crystallographic one present a special type of antiferromagnetism, giving rise to such phenomena as weak ferromagnetism<sup>14</sup>, piezomagnetism<sup>15</sup>, and magnetoelectricity<sup>16</sup>. A

very detailed classification was given by Turov<sup>17,18</sup>, who argued that there are two major classes of unconventional antiferromagnets, depending on whether the spatial inversion  $\mathcal{I}$  enters the magnetic group in combination with  $\mathcal{T}$  or alone. The first scenario corresponds to magnetoelectricity, while the second one, which encompasses weak ferromagnetism and piezomagnetism, has clear similarity to what is now called “altermagnetism”. Canonically, weak ferromagnetism refers to net spin magnetic moments in otherwise AFM substances, while altermagnetism emerged from the analysis of the anomalous Hall effect (AHE)<sup>9,10</sup>. However, from the phenomenological point of view, these two effects are identical to each other: both manifest that  $\mathcal{T}$  is macroscopically broken and the existence of AHE automatically implies the existence of weak ferromagnetism, no matter how “weak” it is. Actually, in his monograph<sup>17</sup>, Turov considered not only weak ferromagnetism, but also AHE and many other phenomena expected in weak ferromagnets. Particularly, already in 1962, Turov and Shavrov predicted that AHE can be induced by AFM order<sup>19</sup>. Apparently, this is the most one can say within phenomenological theories, which do not provide any information about the magnitude of the effect or its microscopic origin.

Despite the fact that AHE is frequently regarded as one of possible manifestations of time-reversal symmetry breaking in altermagnetic systems<sup>2–4</sup>, the aspect of spin splitting in this phenomenon remains to be obscured, and so does the general relation between weak spin ferromagnetism and altermagnetism. The microscopic theory of weak spin ferromagnetism is essentially the theory of Dzyaloshinskii-Moriya (DM) interactions, originally proposed by Moriya for Mott insulators<sup>20</sup> and later extended to a broader class of magnetic systems<sup>21–23</sup>. In this case, the net spin

<sup>1</sup>Research Center for Materials Nanoarchitectonics (MANA), National Institute for Materials Science (NIMS), Tsukuba, Ibaraki, Japan. <sup>2</sup>Department of Materials Engineering Science, The University of Osaka, Toyonaka, Japan. ✉e-mail: [SOLOVYEV.Igor@nims.go.jp](mailto:SOLOVYEV.Igor@nims.go.jp)

magnetization appears at first order in the spin-orbit (SO) coupling, whereas the associated energy change enters at second order. For comparison, the single-ion anisotropy – another source of weak ferromagnetism<sup>24</sup> – produces a net magnetization only in second order and an energy change in fourth order.

Depending on the symmetry, DM interactions can have several components: those that have the same sign in equivalent bonds support weak spin ferromagnetism, while the ones with alternating signs do not contribute to the FM moment or any canting of spins. A notable example is the DM interactions between two magnetic sublattices in CrO<sub>2</sub>, a sister compound of altermagnetic RuO<sub>2</sub>: these interactions are relatively strong but alternate among eight neighbouring bonds<sup>23</sup>. Regarding the role played by the sign-alternating DM interactions, we will argue that they do bear direct and crucial implications for AHE and net orbital magnetization  $\mathcal{M}$ , thus clarifying the fundamental difference between AHE and weak spin ferromagnetism from the microscopic point of view. On the other hand, while the lifting of Kramers spin degeneracy in the non-relativistic limit is regarded to be the central manifestation of breaking  $\mathcal{T}$  in altermagnets<sup>1–3</sup>, we will show that: (i) the bands can remain spin-degenerate even when  $\mathcal{T}$  is broken and (ii) the spin splitting does not play an essential role in the emergence of AHE and  $\mathcal{M}$ , which are driven by relativistic SO interaction.

Finally, in 1997, long before the modern era of altermagnetism, one of us proposed that weak ferromagnets LaMO<sub>3</sub> ( $M = \text{Cr, Mn, and Fe}$ ) can exhibit an appreciable magneto-optical effect (the ac analog of AHE)<sup>25</sup>. Rather than being related to the weak spin ferromagnetism itself, this phenomenon better correlated with the behavior of orbital magnetic moments<sup>25</sup>. Using the modern theory of orbital magnetization<sup>26,27</sup>, we will argue that the conclusion was essentially correct as AHE and  $\mathcal{M}$  have a similar microscopic origin.

## Results

### Lattice symmetry

To be specific, we keep in mind the BO<sub>2</sub> layer of orthorhombic perovskites ABO<sub>3</sub> with the space group  $Pbnm$  or layered perovskites A<sub>2</sub>BO<sub>4</sub> with the space group  $Bmab$ . The characteristic examples are LaFeO<sub>3</sub> and La<sub>2</sub>CuO<sub>4</sub>, forming AFM order in the layer plane ( $xy$ ). There are two magnetic sublattices, centered at the origin  $(0, 0)$  and  $\mathbf{t} = (\frac{1}{2}, \frac{1}{2})$ . The  $Pbnm$  group has four symmetry operations transforming the plane  $xy$  to itself: the unity;  $\mathcal{I}$  about the origin; the twofold rotation about  $x$  combined with the shift by  $\mathbf{t}$ ,  $\{C_{2x}|\mathbf{t}\}$ ; and the mirror reflection of  $x$ , also combined with the shift,  $\{m_x|\mathbf{t}\}$ . In  $Bmab$ , these symmetry operations are combined with the mirror reflection  $m_y$ . Note that, in comparison with the standard setting of the  $Bmab$  group, here we additionally swap the orthorhombic axes  $x$  and  $y$ .  $\{C_{2x}|\mathbf{t}\}$  and  $\{m_x|\mathbf{t}\}$  transform two magnetic sublattices to each other, while  $\mathcal{I}$  and  $m_y$  transform each sublattice to itself.

The phenomenological Landau theory for these and other materials, which were recently considered in ref.<sup>28</sup>, was formulated by Turov<sup>17</sup>, regardless of altermagnetic band splitting. Particularly, he predicted that in these orthorhombic systems, the Néel order along  $x$  gives rise to the weak ferromagnetism along  $z$  and the anomalous Hall response  $\sigma_{xy}$ <sup>17</sup>. Both are linear in the Néel field.

### Model

The microscopic model for the BO<sub>2</sub> layer includes the following ingredients (see Fig. 1): (i) The hoppings between first, second, and third nearest neighbors ( $t_1$ ,  $t_2$ , and  $t_3$ , respectively). (ii) The orthorhombic strain of the second nearest hoppings,  $\delta t_2$ , having the same form in both magnetic sublattices and making the directions  $x$  and  $y$  inequivalent. As we will see, this is a very important parameter, which is responsible for finite values of AHE. (iii) Deformation of the third nearest hoppings,  $\delta t_3$ , alternating between the sublattices 1 and 2, that results in the altermagnetic splitting of bands. (iv) SO coupling in noncentrosymmetric nearest-neighbor bonds, which has the form of spin-dependent hoppings,  $\hat{\mathcal{H}}_{ij}^{\text{so}} = it_{ij} \cdot \hat{\sigma}$ , where  $\hat{\sigma} = (\hat{\sigma}_x, \hat{\sigma}_y, \hat{\sigma}_z)$  is the vector of spin Pauli matrices. The DM interaction,  $\mathbf{D}_{ij}$ , is simply proportional to  $\mathbf{t}_{ij}$  and this universal property holds in insulating<sup>29</sup> as

well as metallic<sup>21–23</sup> regimes. In orthorhombic systems,  $\mathbf{D}_{ij} \sim \mathbf{t}_{ij}$  have the following form around each magnetic site<sup>30</sup>:  $\mathbf{t}_{ij} = (\pm t_x, t_y, t_z)$ , where  $y$  and  $z$  components are the same in all the bonds, while the sign of  $x$  component alternates as shown in Fig. 1c. Thus, if AFM spins are aligned along  $x$ ,  $t_y$  and  $t_z$  are responsible for the weak ferromagnetism along, respectively,  $z$  and  $y$ <sup>31</sup>, while  $t_x$  has no effect on the spin texture. The  $Bmab$  symmetry imposes additional constraints:  $\delta t_3 = 0$  and  $t_z = 0$ . Nevertheless, the band splitting can reappear in the multi-orbital case, considering the hoppings between orbitals belonging to different irreducible representations of the point group.

In conventional antiferromagnets,  $\mathbf{t}$  is the regular translation. Therefore, if magnetic site is in the inversion center, there will be another inversion center between the magnetic sites, meaning that  $\mathbf{D}_{ij} \sim \mathbf{t}_{ij} = 0$ <sup>14,20</sup>.

$\hat{\mathcal{H}}_{ij}^{\text{so}}$  can be eliminated by the SU(2) rotations of the spins,  $\hat{U}_S = e^{-i\varphi \hat{n} \cdot \hat{\sigma}}$ , in the sublattice 2 with  $\mathbf{n} = \frac{\mathbf{t}_{ij}}{|\mathbf{t}_{ij}|}$ ,  $\varphi = 2 \arctan \frac{|t_y|}{t_1}$ , which leads

to the redefinition  $t_1 \rightarrow t_1 \sqrt{1 + \left(\frac{t_y}{t_1}\right)^2}$ <sup>29,32</sup>. However, this transformation depends on the bond and, therefore, cannot be performed simultaneously for all the bonds. Nevertheless, we can still use it to eliminate  $t_y$  and  $t_z$ , but to keep  $t_x$  and  $\hat{\mathcal{H}}_{ij}^{\text{so}} = \pm it_x \hat{\sigma}_x$ . The corresponding transformation is given by  $\hat{U}_S$  with  $t_x = 0$ . Therefore, the parameters  $t_y$  and  $t_z$ , which are responsible for weak spin ferromagnetism, do not play any role in AHE and orbital magnetization. Finally, we add the Néel field  $\pm B \hat{\sigma}_x$  along  $x$ , which yields FM moment along  $z$ <sup>31</sup>. Then, after global rotation of spins, transforming  $\hat{\sigma}_x$  to  $\hat{\sigma}_z$ , we will have the following  $4 \times 4$  Hamiltonian<sup>33</sup>, which is diagonal with respect to spins  $\sigma = \pm$ :

$$\hat{\mathcal{H}}_k = h_k - \delta h_k^3 \hat{\tau}_z + h_k^1 \hat{\tau}_x - B \hat{\tau}_z \hat{\sigma}_z - h_k^{\text{so}} \hat{\tau}_y \hat{\sigma}_z, \quad (1)$$

where two AFM sublattices are described in terms of Pauli matrices  $\hat{\tau} = (\hat{\tau}_x, \hat{\tau}_y, \hat{\tau}_z)$ <sup>33</sup>,  $h_k = h_k^2 + \delta h_k^2 + h_k^3$ ,  $h_k^2 = 2t_2(\cos k_x + \cos k_y)$ ,  $\delta h_k^2 = \delta t_2(\cos k_x - \cos k_y)$ ,  $h_k^3 = 4t_3 \cos k_x \cos k_y$ ,  $\delta h_k^3 = 4\delta t_3 \sin k_x \sin k_y$ ,  $h_k^1 = 4t_1 \cos \frac{k_x}{2} \cos \frac{k_y}{2}$ , and  $h_k^{\text{so}} = 4t_x \sin \frac{k_x}{2} \sin \frac{k_y}{2}$ .

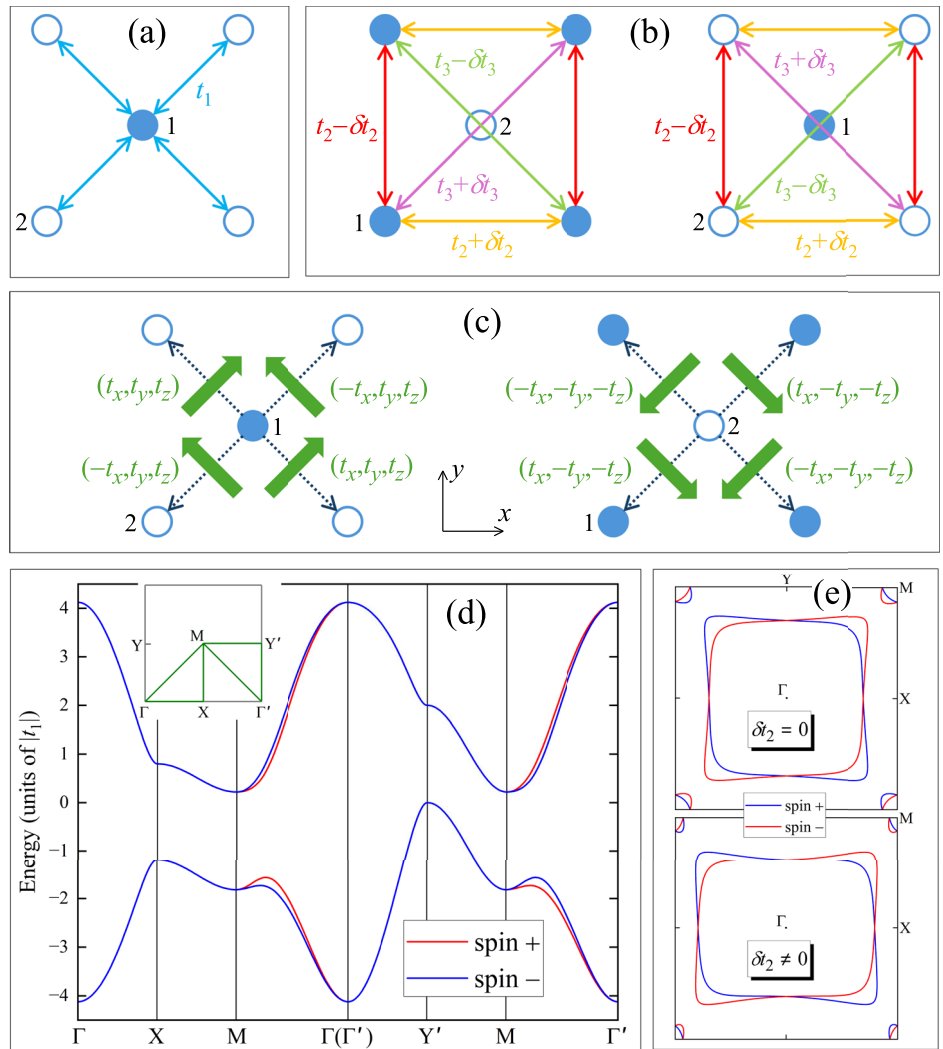
The model parameters can be derived from DFT<sup>34–37</sup>, as we will do below for La<sub>2</sub>CuO<sub>4</sub>. Alternatively, one can take the exchange interactions,  $J_k$ , and evaluate the parameters from the superexchange theory as  $|t_k/t_1| = \sqrt{J_k/J_1}$  and  $2t_y/t_1 = \mathbf{D}_{ij}/J_1$ <sup>29</sup>.  $\delta t_2$  and  $\delta t_3$  can be exceptionally large in orthorhombic manganites, to facilitate the formation of spin-spiral multiferroic phases<sup>23</sup>. Note that the large  $\delta t_3$  arises from the Jahn-Teller distortion, while the SO-induced term  $t_x$  is associated with the tilting of the BO<sub>6</sub> octahedra. A reasonable choice is (in units of  $t_1 < 0$ ):  $t_3 \sim -t_2 \sim 0.1$  and  $\delta t_3 \sim t_x \sim -\delta t_2 \sim 0.05$ <sup>23</sup>, which will be used unless it is specified otherwise.  $|B| = 1$  is sufficient to open the band gap. Examples of such band structure,  $\epsilon_{k,v}^{\sigma} = h_k + v\sqrt{(\sigma B + \delta h_k^3)^2 + (h_k^1)^2 + (h_k^{\text{so}})^2}$  ( $v = \pm$  being the band index), and Fermi surface are shown in Fig. 1(d),(e). As expected,  $\delta t_3$  splits the bands, while  $\delta t_2$  deforms the Fermi surface.

Similar model has been considered by Naka et al. for the analysis of AHE in  $\kappa$ -type organic antiferromagnets<sup>8,10</sup>, obeying the same orthorhombic symmetry, who arrived to similar conclusions: crucial importance of sign-alternating part of SO interaction and orthorhombic strain, and relative unimportance of altermagnetic band splitting. These conclusions have been further supported by the analysis of more sophisticated multi-orbital model for orthorhombic perovskites<sup>38</sup>.

### Hidden symmetries

A very interesting situation occurs when  $\delta t_3 = 0$  (i.e., *without altermagnetic splitting of bands*). Since  $\mathcal{T} \hat{\sigma}_z = -\hat{\sigma}_z$ , the Néel field  $B \hat{\tau}_z \hat{\sigma}_z$  breaks  $\mathcal{T}$ , but remains invariant under  $\{\mathcal{T}|\mathbf{t}\}$ , where  $\mathcal{T}$  is combined with the lattice shift of site 1 to site 2 (and vice versa), which additionally changes  $\hat{\tau}_z$  to  $-\hat{\tau}_z$ . Then, since  $B \hat{\tau}_z \hat{\sigma}_z$  is real and  $\mathcal{T} = \mathcal{S}K$ , where  $K$  is the complex conjugation and  $\mathcal{S} = i\hat{\sigma}_y$  flips  $\sigma$  to  $-\sigma$ ,  $\mathcal{T}$  can be replaced by  $\mathcal{S}$ , so that the Néel field is also invariant under  $\{\mathcal{S}|\mathbf{t}\} \equiv i\hat{\sigma}_y \hat{\tau}_x$ . On the other

**Fig. 1 | Parameters and basic electronic structure.** Hopping parameters between (a) first nearest neighbors and (b) second and third nearest neighbors. c Parameters of spin-orbit interaction around two magnetic sites (denotes as 1 and 2). The directions of the bonds are shown by dotted arrows. d Example of band structure. The inset shows high-symmetry points of the Brillouin zone. e Corresponding Fermi surface for  $n_{\text{el}} = 1$  with and without orthorhombic strain  $\delta t_2 = 0.15$ .



hand, the spin-orbit interaction,  $h_k^{\text{so}} \hat{\tau}_y \hat{\sigma}_z$ , is invariant under  $\mathcal{T}$ , but changes its sign when it is combined with the lattice shift,  $\{\mathcal{T}|\mathbf{t}\}$ . However, since  $\hat{\tau}_y$  is complex, this sign change does not occur if one uses  $\{S|\mathbf{t}\}$  instead of  $\{\mathcal{T}|\mathbf{t}\}$ . Therefore, the spin-orbit interaction is invariant under  $\{S|\mathbf{t}\}$ , so as the full Hamiltonian (1). This means that eigenstates with  $\sigma = \pm$  differ only by a phase factor. The latter guarantees that (i) the  $\sigma = \pm$  bands are degenerate and (ii) the contributions of these bands to  $\sigma_{xy}$  are equal to each other and, instead of the partial cancellation, which would occur in ferromagnets, we have an *addition* of such contributions.

Importantly, the  $\{S|\mathbf{t}\}$  symmetry is a consequence of inversional invariance (the “centrosymmetric antiferromagnetism” in the definition of Turov<sup>17,39</sup>). This is an interesting example of intertwined fundamental properties of matter, when  $\mathcal{I}$  controls the properties related to time-reversal symmetry breaking.

### Berry curvature and AHE

$\sigma_{xy}$  is given by the Brillouin zone (BZ) integral of the Berry curvatures,  $\Omega_k^{\sigma 40,41}$  (in atomic units):

$$\sigma_{xy} = - \int_{\text{BZ}} \frac{d\mathbf{k}}{(2\pi)^2} \sum_{\sigma=\pm} f_k^{\sigma} \Omega_k^{\sigma}, \quad (2)$$

where  $f_k^{\sigma}$  is Fermi-Dirac distribution function and  $\Omega_k^{\sigma} = -2\text{Im}(\partial_{k_x} u_k^{\sigma} | \partial_{k_y} u_k^{\sigma})$ . Without loss of generality, one can consider the case where  $\nu = -$  bands are partially occupied by  $n_{\text{el}}$  electrons while  $\nu = +$

bands are empty. Searching eigenvectors for  $\nu = -$  in the form:

$$|u_k^{\sigma}\rangle = \begin{pmatrix} \cos \theta_k^{\sigma} e^{i\phi_k^{\sigma}} \\ \sin \theta_k^{\sigma} \end{pmatrix}, \quad (3)$$

it is straightforward to find (Supplementary, Sec. A):

$$\theta_k^{\sigma} = -\frac{1}{2} \arctan \frac{\sqrt{(h_k^1)^2 + (h_k^{\text{so}})^2}}{\sigma B + \delta h_k^3} \quad (4)$$

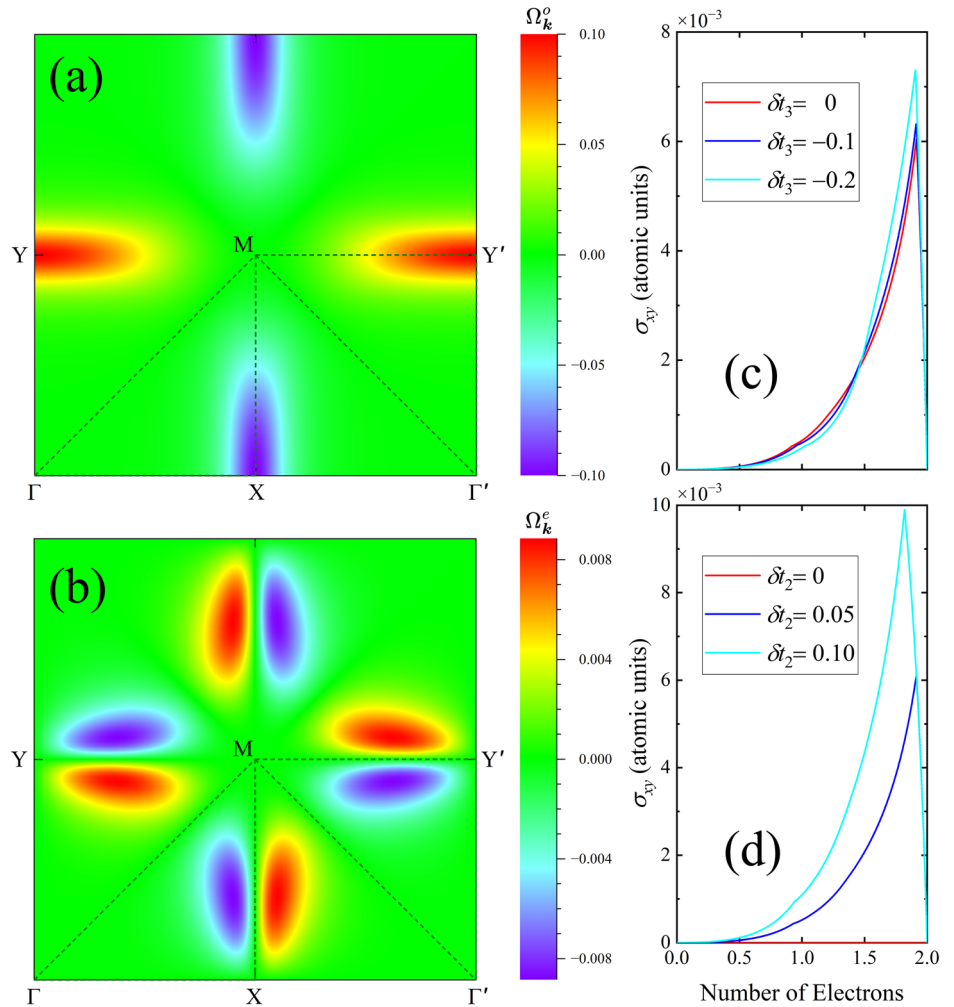
( $0 \leq \theta_k^{\sigma} < \pi$ ) and  $\phi_k^{\sigma} = \sigma \arctan(h_k^{\text{so}}/h_k^1)$  ( $0 \leq \phi_k^{\sigma} < 2\pi$ ), which are, respectively, even and odd in  $t_x$  (SO coupling). Therefore, the Berry curvature, which can be expressed as the cross product,  $\Omega_k^{\sigma} = \sin 2\theta_k^{\sigma} [\partial_{k_x} \theta_k^{\sigma} \times \partial_{k_y} \theta_k^{\sigma}]_z$ , is odd in  $t_x$ . Since  $\sin 2\theta_k^{\sigma} \partial_{k_x} \theta_k^{\sigma} = -\frac{1}{2} \partial_{k_x} (\cos 2\theta_k^{\sigma})$ ,  $\sigma_{xy}$  can be reformulated in terms of group velocities,  $\partial_{k_x} \varepsilon_k^{\sigma}$ , at the Fermi surface (Supplementary, Sec. B):

$$\sigma_{xy} = -\frac{1}{2} \int_{\text{BZ}} \frac{d\mathbf{k}}{(2\pi)^2} \sum_{\sigma=\pm} \frac{\partial f_k^{\sigma}}{\partial \varepsilon_k^{\sigma}} \cos 2\theta_k^{\sigma} [\partial_{k_x} \varepsilon_k^{\sigma} \times \partial_{k_y} \varepsilon_k^{\sigma}]_z, \quad (5)$$

as was generally pointed out by Haldane<sup>42</sup>.

If  $\delta t_3$  is finite,  $\Omega_k^{\sigma}$  contains both odd and even components in  $B$ , that immediately follows from the form of  $\theta_k^{\sigma}$ . Thus, one can write  $\Omega_k^{\pm} = \Omega_k^{\text{o}} \pm \Omega_k^{\text{e}}$ , where  $\Omega_k^{\text{o}}$  and  $\Omega_k^{\text{e}}$  are, respectively, odd and even in  $B$ . Here,

**Fig. 2 | Anomalous Hall effect.** (a) odd ( $\Omega_k^o$ ) and (b) even ( $\Omega_k^e$ ) components of the Berry curvature. Band-filling dependence of  $\sigma_{xy}$  for different values of (c)  $\delta t_3$  and (d)  $\delta t_2$ .



we used that  $\Omega_k^-$  can be obtained from  $\Omega_k^+$  by changing the signs of both  $B$  and  $t_x$ , which follows from the form of  $\hat{\mathcal{H}}_k$ . This yields  $\sigma_{xy} = \sigma_{xy}^I + \sigma_{xy}^{II}$  with

$$\sigma_{xy}^I = - \int_{\text{BZ}} \frac{d\mathbf{k}}{(2\pi)^2} (f_k^+ + f_k^-) \Omega_k^o \quad (6)$$

and

$$\sigma_{xy}^{II} = - \int_{\text{BZ}} \frac{d\mathbf{k}}{(2\pi)^2} (f_k^+ - f_k^-) \Omega_k^e, \quad (7)$$

where  $(f_k^+ + f_k^-)$  and  $(f_k^+ - f_k^-)$  are, respectively, even and odd in  $B$ . Thus, both  $\sigma_{xy}^I$  and  $\sigma_{xy}^{II}$  are odd in  $B$ .  $\sigma_{xy}^{II}$  is caused by the altermagnetic splitting of bands and is finite only when the band with one spin is occupied, while the band with opposite spin is empty. This is somewhat similar to ferromagnets, where AHE is caused by imperfect compensation between contributions with different spins. More intriguing is the existence of finite  $\sigma_{xy}^I$  in case of spin-degenerate bands due to special symmetry of the Hamiltonian (1), as was discussed above.

### Large- $B$ limit

More insight can be gained by considering  $\Omega_k^o$  and  $\Omega_k^e$  in the limit of large  $B$  (Supplementary, Sec. B3):

$$\Omega_k^o \approx \frac{2t_1 t_x}{B|B|} \left( \frac{t_1^2 - t_x^2 \tan^2 \frac{k_x}{2}}{t_1^2 + t_x^2 \tan^2 \frac{k_x}{2} \tan^2 \frac{k_y}{2}} \sin^2 \frac{k_y}{2} - k_x \leftrightarrow k_y \right) \quad (8)$$

and

$$\Omega_k^e \approx -2 \frac{\delta t_3^2}{B} \Omega_k^o + \frac{4t_1 t_x \delta t_3}{|B|^3} (\sin k_x \sin 2k_y - k_x \leftrightarrow k_y). \quad (9)$$

(i) The altermagnetic contribution  $\Omega_k^e$ , which is proportional to  $\delta t_3$ , is expected to be smaller than  $\Omega_k^o$  by the factor  $\frac{|\delta t_3|}{B}$ . (ii) Both terms are antisymmetric with respect to the permutation of  $k_x$  and  $k_y$ . Therefore,  $\sigma_{xy}$ , given by the BZ integral, will vanish unless there is some “anisotropy”, discriminating between  $k_x$  and  $k_y$ . The role of this anisotropy is played by the orthorhombic strain  $\delta t_2$ . The Berry curvature itself does not depend on  $\delta t_2$ . However,  $\delta t_2$  deforms the Fermi surface [Fig. 1e], and thus yields finite  $\sigma_{xy}$ . Although the term “orthorhombic strain” is relevant to one particular type of lattice, the idea itself is much more general. For instance, in  $\text{RuO}_2$  we deal with the  $\sigma_{zx}$  component instead of  $\sigma_{xy}$ . Therefore, this is the tetragonal distortion,  $c/a$ , which plays the same role and is responsible for finite  $\sigma_{zx}$  in  $\text{RuO}_2$ .<sup>39</sup>

The behavior of Berry curvature and  $\sigma_{xy}$  is summarized in Fig. 2.  $\Omega_k^o$  and  $\Omega_k^e$  have nodes along  $\Gamma$ -M- $\Gamma'$ . Moreover,  $\Omega_k^e$  has additional nodes along X-M-Y', as can be also clearly seen from the above expressions in the large- $B$  limit. The magnitude of  $\Omega_k^e$  is generally smaller, which is again consistent with the above estimate for large  $B$ . The actual contribution of  $\Omega_k^e$  to  $\sigma_{xy}$  is even smaller because the largest band splitting is expected along  $\Gamma$ -M- $\Gamma'$  [Fig. 1(d),(e)], which is the nodeline of  $\Omega_k^e$ . Therefore, for realistic values  $|\delta t_3| \lesssim |t_3|$ , the contribution of  $\Omega_k^e$  to  $\sigma_{xy}$  is practically negligible. Furthermore,  $|\Omega_k^o|$  is the largest along X-M-Y', where the bands are spin-degenerate. On the other hand,  $\sigma_{xy}$  rises rapidly with the increase of  $\delta t_2$ . The kink of  $\sigma_{xy}$  around  $n_{\text{el}} = 1.9$  is related to the depopulation of states near the X



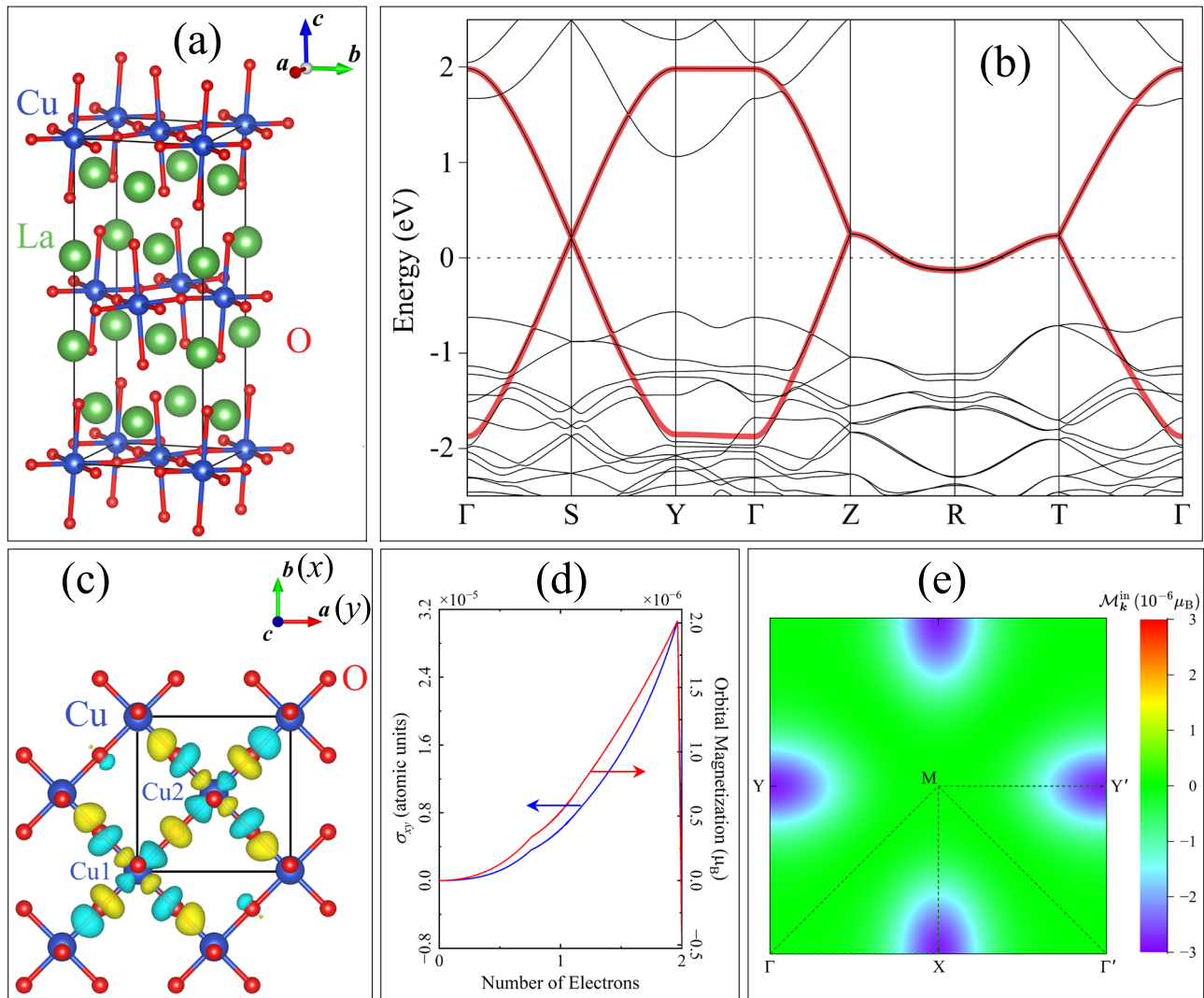


**Fig. 3 | Construction of realistic model for  $\text{La}_2\text{CuO}_4$ .** **a** Crystal structure. **b** Electronic structure near the Fermi level. The red line shows the tight-binding dispersion of the  $x^2$ - $y^2$  band. **c** Corresponding Wannier functions. **d** Band-filling

dependence of  $\sigma_{xy}$  and orbital magnetization. **e** The integrand,  $\mathcal{M}_k^{\text{in}}$ , specifying the orbital magnetization in the insulating state for  $n_{\text{el}} = 2$  electrons.

point, which are lower in energy than the ones in the Y (Y') point due to the orthorhombic strain.

We would like to emphasize that although  $\Omega_k^o$  and  $\Omega_k^e$  can be considered independently, both contributions are proportional to  $t_x$  and driven by relativistic SO interaction. Therefore, there is no AHE without SO interaction. Conversely, a finite AHE can exist even in the absence of band splitting  $\delta t_3$ . In the latter case, it is given solely by  $\Omega_k^o$ .

### Orbital magnetization

$\mathcal{M}$  is given by the BZ integral of

$$\mathcal{M}_k^o = \text{Im} \langle \partial_{k_x} u_k^\sigma | \hat{\mathcal{H}}_k^\sigma | u_k^\sigma \rangle + \epsilon_k^\sigma - 2\mu | \partial_{k_y} u_k^\sigma \rangle \quad (10)$$

(per two sites), where  $\mu$  is the chemical potential<sup>26,27</sup>. Introducing  $\mathcal{M}_k^\pm = \mathcal{M}_k^o \pm \mathcal{M}_k^e$ , one can identify two contributions,  $\mathcal{M} = \mathcal{M}^I + \mathcal{M}^{II}$ , similar to AHE (Supplementary, Sec. C). In the insulating state for  $n_{\text{el}} = 2$ , it is sufficient to consider only the orthorhombic strain part of  $\hat{\mathcal{H}}_k^\sigma$  and  $\epsilon_k^\sigma$ . Then,  $\mathcal{M}$  is given by the BZ integral of  $\mathcal{M}_k^{\text{in}} = -2\delta h_k^2 \Omega_k^o$ .

### The case of $\text{La}_2\text{CuO}_4$

The simplest realistic model for  $\text{La}_2\text{CuO}_4$  can be constructed for the  $x^2$ - $y^2$  band near the Fermi level, as suggested by DFT calculations, and

using for these purposes Wannier functions technique<sup>34,35</sup> (Fig. 3).  $2B \approx U$  (the on-site Coulomb repulsion) can be evaluated from constrained random phase approximation<sup>36,37</sup>. It yields the following parameters (see Methods):  $U = 2.196$  eV,  $t_1 = -439.02$  meV,  $t_2 = 34.07$  meV,  $\delta t_2 = 5.06$  meV,  $t_3 = -30.27$  meV,  $t_x = -1.27$  meV, and  $t_y = -3.70$  meV.  $\mathcal{M}$  replicates the shape of  $\sigma_{xy}$ , including the kink position [Fig. 3d]. This is to be expected: for the narrow-band compounds, the  $\mathbf{k}$ -dispersion of  $\hat{\mathcal{H}}_k^\sigma$  and  $\epsilon_k^\sigma$  is relatively weak and, therefore,  $\mathcal{M}_k^\sigma \sim \Omega_k^{\sigma 43}$ . Nevertheless, the  $\mathbf{k}$ -dispersion of  $\delta h_k^2$  additionally modulates the sign-alternating  $\Omega_k^o$  along X–Y', thus making  $\mathcal{M}_k^{\text{in}} \leq 0$  throughout the BZ [Fig. 3(e)] and causing  $\mathcal{M}$  to be finite. This can be viewed as a piezomagnetism induced by the orthorhombic strain.

The numerical value of  $\mathcal{M}$  is small ( $\sim 5 \times 10^{-7} \mu_B$ ), but finite. It should be noted that the orbital magnetism in the one-orbital model is purely itinerant, as it is caused by intersite processes. The additional, single-site contribution to  $\mathcal{M}$  can emerge in the more general multi-orbital framework<sup>25</sup>. However, for the  $e_g$  states in  $\text{La}_2\text{CuO}_4$ , this contribution is also small, as it is induced by interactions with occupied  $t_{2g}$  states, which are largely separated from the  $e_g$  ones. Thus,  $\mathcal{M}$  is expected to be smaller than spin net magnetic moment  $8St_y/t_1 \sim 0.03 \mu_B$ , where  $S = \frac{1}{2}$ , meaning that  $\text{La}_2\text{CuO}_4$  is the canonical weak spin ferromagnet. Nevertheless, this situation is not generic and there are indeed cases where the spin net magnetic

moment can vanish, as expected from the form of DM interactions in  $\text{RuO}_2$ <sup>23</sup>. Then, what is the proper order parameter classifying such unconventional AFM state<sup>44,45</sup>? We believe that the legitimate choice is  $\mathcal{M}$ <sup>25</sup>. Similar to AHE, it is ultimately related to the Berry curvature and induced by sign-alternating part of the SO coupling. Furthermore, although being typically small, it remains finite (unlike spin net magnetic moment) and in many respects replicates the behavior of AHE. In  $\text{RuO}_2$  and other AFM rutile compounds, the net spin magnetization can be induced by single-ion anisotropy<sup>24</sup>. However, this contribution is second order in the SO coupling, whereas  $\mathcal{M}$  appears already at first order.

## Discussion

Altermagnetism presents a new turn in the development of weak ferromagnetism, bringing the analysis to the microscopic level and, thus, revealing new aspects in old-standing problems. Although from a phenomenological point of view the phenomena of weak ferromagnetism and AHE are basically identical, the microscopic pictures behind them are different and can be linked to, respectively, nonalternating and alternating in sign DM interactions. Nevertheless, these components typically coexist as both of them are induced by the same oxygen displacements, tending to align the DM vectors perpendicular to magnetic bonds<sup>46</sup>. This is the reason why weak spin ferromagnetism and AHE frequently coexist and cannot be easily separated<sup>47</sup>. In this respect, we show that, as these phenomena have different microscopic origin, they should be separable.

The altermagnetic band splitting does not play a key role in AHE. The  $\{S|t\}$  symmetry of the microscopic Hamiltonian supports the spin degeneracy of the bands, but does not exclude breaking of  $\mathcal{T}$ . The lack of the band splitting, which was recently observed in some potential altermagnets<sup>48</sup>, does not necessarily mean the absence of AHE. Although the altermagnetic band splitting is allowed by symmetry, the symmetry itself does not say anything about whether it is large or small. It can be accidentally zero or even forbidden for certain symmetries, as in  $\text{La}_2\text{CuO}_4$ . On the other hand, the relativistic SO interaction, which is mainly responsible for AHE and  $\mathcal{M}$  in such unconventional antiferromagnets is always finite owing to a lack of bond inversion symmetry.

Furthermore, the  $\{S|t\}$  symmetry imposes a constraint on the form of SO interactions, which allows us to perform a transformation to some local coordinate frame, where unconventional antiferromagnet with the SO interaction can be described as a ferromagnet with only one magnetic site per cell<sup>39</sup>. This solves the puzzle of why some nearly collinear antiferromagnets can exhibit simultaneously AHE and  $\mathcal{M}$  – two quantities, having the same microscopic origin and displaying similar behavior, when the existence of AHE automatically means the existence of  $\mathcal{M}$  and vice versa.

The orthorhombic strain, which is typically ignored in models of altermagnetism<sup>33,49</sup>, is another key ingredient responsible for finite AHE and  $\mathcal{M}$  in analogy with piezomagnetism.

## Methods

### Details of electronic-structure calculations for $\text{La}_2\text{CuO}_4$

We adopt the orthorhombic *Bmab* crystal structure of  $\text{La}_2\text{CuO}_4$ , as shown in Fig. 3a<sup>50</sup>. Electronic structure calculations were performed within DFT using generalized gradient approximation (GGA) for the exchange-correlation potential<sup>51</sup> with spin-orbit coupling as implemented in the Quantum-ESPRESSO package, using ultrasoft pseudopotentials<sup>52</sup>. Energy cutoff for wavefunctions and charge density was set to 80 Ry and 80 Ry, respectively. The Brillouin zone was sampled by a  $12 \times 12 \times 16$  Monkhorst-Pack mesh<sup>53</sup>, and the total energy convergence criterion was put to  $10^{-9}$  Ry. The results are also verified using local density approximation as implemented in the VASP package<sup>54,55</sup>.

The one-orbital model for the Cu states is constructed in the basis of Wannier functions using the procedure of maximal localization as implemented in the wannier90 package<sup>34,35</sup>. The Wannier functions were calculated by projecting the states near the Fermi level in the range of  $[-2.5, 2.5]$  eV onto the atomic  $x^2-y^2$  orbitals. The states in the range of  $[-0.2,$

$1.0]$  eV with respect to the Fermi level were kept fixed. The on-site Coulomb interaction was calculated within the constrained random phase approximation<sup>36</sup>, as implemented in the RESPACK package<sup>37</sup> using norm-conserving pseudopotentials without spin-orbit coupling. Energy cutoff for wavefunctions and charge density was set to 100 Ry and 400 Ry, respectively, and the Brillouin zone was sampled by a  $8 \times 8 \times 10$  Monkhorst-Pack mesh.

$t_y$  appears to be sensitive to the choice of the local coordinate frame, which was necessary for specifying the  $x^2-y^2$  Wannier functions. We believe it is more appropriate to use the same coordinate frame at both Cu sites, which yields  $t_y = -3.70$  meV. Alternatively, one can align the  $z$  axes along the apical oxygen sites, which are slightly rotated relative to each other at two Cu sites. This yields  $t_y = -6.57$  meV. Such ambiguity is related to the fact that SO coupling parameters depend on the unitary transformation  $e^{-i\varphi'\mathbf{n}'\cdot\boldsymbol{\sigma}}$ <sup>29,32</sup>, where  $\varphi'$  and  $\mathbf{n}'$  are specified by the choice of the local coordinate frame. The interlayer hoppings are about 5 meV and have been neglected.

## Data Availability

The data supporting the findings of this study are available within this article. Additional data are available from the corresponding author on reasonable request.

Received: 15 January 2026; Accepted: 13 May 2026;

Published online: 22 May 2026

## References

- Šmejkal, L., Sinova, J. & Jungwirth, T. Beyond conventional ferromagnetism and antiferromagnetism: a phase with nonrelativistic spin and crystal rotation symmetry. *Phys. Rev. X* **12**, 031042 (2022).
- Šmejkal, L., Sinova, J. & Jungwirth, T. Emerging research landscape of altermagnetism. *Phys. Rev. X* **12**, 040501 (2022).
- Bai, L. et al. Altermagnetism: exploring new frontiers in magnetism and spintronics. *Adv. Funct. Mater.* **34**, 2409327 (2024).
- Naka, M., Motome, Y. & Seo, H. Altermagnetic perovskites. *npj Spintronics* **3**, 1 (2025).
- Noda, Y., Ohno, K. & Nakamura, S. Momentum-dependent band spin splitting in semiconducting  $\text{MnO}_2$ : a density functional calculation. *Phys. Chem. Chem. Phys.* **18**, 13294 (2016).
- Okugawa, T., Ohno, K., Noda, Y. & Nakamura, S. Weakly spin-dependent band structures of antiferromagnetic perovskite  $\text{LaMO}_3$  ( $M = \text{Cr}, \text{Mn}, \text{Fe}$ ). *J. Phys.: Condens. Matter* **30**, 075502 (2018).
- Hayami, S., Yanagi, Y. & Kusunose, H. Momentum-Dependent Spin Splitting by Collinear Antiferromagnetic Ordering. *J. Phys. Soc. Jpn* **88**, 123702 (2019).
- Naka, M. et al. Spin current generation in organic antiferromagnets. *Nat. Commun.* **10**, 4305 (2019).
- Šmejkal, L., González-Hernández, R., Jungwirth, T. & Sinova, J. Crystal time-reversal symmetry breaking and spontaneous Hall effect in collinear antiferromagnets. *Sci. Adv.* **6**, eaaz8809 (2020).
- Naka, M. et al. Anomalous Hall effect in  $\kappa$ -type organic antiferromagnets. *Phys. Rev. B* **102**, 075112 (2020).
- Ma, H.Y. et al. Multifunctional antiferromagnetic materials with giant piezomagnetism and noncollinear spin current. *Nat. Commun.* **12**, 2846 (2021).
- Streltsov, S. V. & Cheong, S.-W. Altermagnetism in 6H perovskites. *npj Quantum Mater.* **10**, 102 (2025).
- Dzyaloshinskii, I. E. Space and time parity violation in anyonic and chiral systems. *Phys. Lett. A* **155**, 62 (1991).
- Dzyaloshinsky, I. A thermodynamic theory of “weak” ferromagnetism of antiferromagnetics. *J. Chem. Phys. Solids* **4**, 241 (1958).
- Dzyaloshinskii, I. E. The problem of piezomagnetism. *JETP (USSR)* **6**, 621 (1958).
- Dzyaloshinskii, I. E. On the magneto-electrical effect in antiferromagnets. *JETP (USSR)* **10**, 628 (1960).

17. Turov, E. A., Kinetic, optical, and acoustic properties of antiferromagnets (Ural Division of Academy of Sciences of the USSR, 1990).
18. Turov, E. A. Can the magnetoelectric effect coexist with weak piezomagnetism and ferromagnetism? *Phys.-Uspekhi (USSR)* **37**, 303–310 (1994).
19. Turov, E. A. & Shavrov, V. G. On some galvano- and thermomagnetic effects in antiferromagnets. *JETP (USSR)* **16**, 1606 (1963).
20. Moriya, T. Anisotropic Superexchange Interaction and Weak Ferromagnetism. *Phys. Rev.* **120**, 91 (1960).
21. Katsnelson, M. I., Kvashnin, Y. O., Mazurenko, V. V. & Lichtenstein, A. I. Correlated band theory of spin and orbital contributions to Dzyaloshinskii-Moriya interactions. *Phys. Rev. B* **82**, 100403(R) (2010).
22. Kikuchi, T., Koretsune, T., Arita, R. & Tatara, G. Dzyaloshinskii-Moriya interaction as a consequence of a doppler shift due to spin-orbit-induced intrinsic spin current. *Phys. Rev. Lett.* **116**, 247201 (2016).
23. Solovyev, I. V. Linear response theories for interatomic exchange interactions. *J. Phys.: Condens. Matter* **36**, 223001 (2024).
24. Moriya, T. Theory of Magnetism of  $\text{NiF}_2$ . *Phys. Rev.* **117**, 635 (1960).
25. Solovyev, I. V. Magneto-optical effect in the weak ferromagnets  $\text{LaMO}_3$  ( $M = \text{Cr, Mn, and Fe}$ ). *Phys. Rev. B* **55**, 8060 (1997).
26. Thonhauser, T., Ceresoli, D., Vanderbilt, D. & Resta, R. Orbital magnetization in periodic insulators. *Phys. Rev. Lett.* **95**, 137205 (2005).
27. Shi, J., Vignale, G., Xiao, D. & Niu, Q. Quantum theory of orbital magnetization and its generalization to interacting systems. *Phys. Rev. Lett.* **99**, 197202 (2007).
28. McClarty, P. A. & Rau, J. G. Landau Theory of Altermagnetism. *Phys. Rev. Lett.* **132**, 176702 (2024).
29. Shekhtman, L., Entin-Wohlman, O. & Aharony, A. Moriya's anisotropic superexchange interaction, frustration, and Dzyaloshinsky's weak ferromagnetism. *Phys. Rev. Lett.* **69**, 836 (1992).
30. Solovyev, I., Hamada, N. & Terakura, K. Crucial Role of the Lattice Distortion in the Magnetism of  $\text{LaMnO}_3$ . *Phys. Rev. Lett.* **76**, 4825 (1996).
31. Yamaguchi, T. & Tsushima, K. Magnetic symmetry of rare-earth orthochromites and orthoferrites. *Phys. Rev. B* **8**, 5187 (1973).
32. Kaplan, T. A. Single-Band Hubbard Model with Spin-Orbit Coupling. *Z. Phys. B* **49**, 313 (1983).
33. Roig, M., Kreisel, A., Yu, Y., Andersen, B. M. & Agterberg, D. F. Minimal models for altermagnetism. *Phys. Rev. B* **110**, 144412 (2024).
34. Marzari, N., Mostofi, A. A., Yates, J. R., Souza, I. & Vanderbilt, D. Maximally localized Wannier functions: Theory and applications. *Rev. Mod. Phys.* **84**, 1419 (2012).
35. Mostofi, A. A. et al. An updated version of Wannier90: A tool for obtaining maximally-localised Wannier functions. *Comput. Phys. Commun.* **185**, 2309 (2014).
36. Aryasetiawan, F. et al. Frequency-dependent local interactions and low-energy effective models from electronic structure calculations. *Phys. Rev. B* **70**, 195104 (2004).
37. Nakamura, K. et al. RESPACK: An ab initio tool for derivation of effective low-energy model of material. *Computer Phys. Commun.* **261**, 107781 (2021).
38. Naka, M., Motome, Y. & Seo, H. Anomalous Hall effect in antiferromagnetic perovskites. *Phys. Rev. B* **106**, 195149 (2022).
39. Solovyev, I. V. Hidden ferromagnetism of centrosymmetric antiferromagnets. *arXiv:2509.00369* (2025).
40. Fang, Z. et al. The anomalous Hall effect and magnetic monopoles in momentum space. *Science* **302**, 92 (2003).
41. Yao, Y. et al. First principles calculation of anomalous Hall conductivity in ferromagnetic bcc Fe. *Phys. Rev. Lett.* **92**, 037204 (2004).
42. Haldane, F. D. M. Berry curvature on the Fermi surface: anomalous Hall effect as a topological Fermi-liquid property. *Phys. Rev. Lett.* **93**, 206602 (2004).
43. Nikolaev, S. A. & Solovyev, I. V. Orbital magnetization of insulating perovskite transition-metal oxides with a net ferromagnetic moment in the ground state. *Phys. Rev. B* **89**, 064428 (2014).
44. Sato, T. & Hayami, S., Quantum theory of magnetic octupole in periodic crystals and characterization of time-reversal-symmetry breaking antiferromagnetism. *arXiv:2504.21431* (2025).
45. Ôiké, J., Peters, R. & Shinada, K. Thermodynamic formulation of the spin magnetic octupole moment in bulk crystals. *Phys. Rev. B* **112**, 134412 (2025).
46. Keffer, F. Moriya Interaction and the Problem of the Spin Arrangements in  $\beta\text{MnS}$ . *Phys. Rev.* **126**, 896 (1962).
47. Hariki, A., Sakurai, K., Okauchi, T. & Kuneš, J. Separating altermagnetic and ferromagnetic effects in X-ray magnetic dichroism of rutile  $\text{NiF}_2$ . *npj Quantum Mater.* **10**, 49 (2025).
48. Morano, V. C. et al. Absence of altermagnetic magnon band splitting in  $\text{MnF}_2$ . *Phys. Rev. Lett.* **134**, 226702 (2025).
49. Maier, T. A. & Okamoto, S. Weak-coupling theory of neutron scattering as a probe of altermagnetism. *Phys. Rev. B* **108**, L100402 (2023).
50. Reehuis, M. et al. Crystal structure and high-field magnetism of  $\text{La}_2\text{CuO}_4$ . *Phys. Rev. B* **73**, 144513 (2006).
51. Perdew, J. P., Burke, K. & Ernzerhof, M. Generalized Gradient Approximation Made Simple. *Phys. Rev. Lett.* **77**, 3865 (1996).
52. Giannozzi, P. et al. Quantum ESPRESSO: a modular and open-source software project for quantum simulations of materials. *J. Phys.: Condens. Matter* **21**, 395502 (2009).
53. Monkhorst, H. J. & Pack, J. D. Special points for Brillouin-zone integrations. *Phys. Rev. B* **13**, 5188 (1976).
54. Kresse, G. & Joubert, D. From ultrasoft pseudopotentials to the projector augmented-wave method. *Phys. Rev. B* **59**, 1758 (1999).
55. Kresse, G. & Furthmüller, J. Efficient iterative schemes for ab initio total-energy calculations using a plane-wave basis set. *Phys. Rev. B* **54**, 11169 (1996).

## Acknowledgements

We are grateful to M. Naka, H. Seo, and A. Lichtenstein for valuable comments and discussions, M. Katsnelson for drawing our attention to the book [16], and A. Katanin and S. Streltsov for providing a copy of this book. MANA is supported by World Premier International Research Center Initiative (WPI), MEXT, Japan. This research did not receive funding.

## Author contributions

I.S. conceptualized the work, performed the calculations (except specified below), and wrote the manuscript. S.N. performed electronic structure calculations and constructed model Hamiltonian for  $\text{La}_2\text{CuO}_4$ . S.N. and A.T. discussed the results and commented on the manuscript. All authors reviewed the manuscript.

## Competing interests

The authors declare no competing interests.

## Additional information

**Supplementary information** The online version contains supplementary material available at <https://doi.org/10.1038/s41535-026-00900-9>.

**Correspondence** and requests for materials should be addressed to Igor Solovyev.

**Reprints and permissions information** is available at <http://www.nature.com/reprints>

**Publisher's note** Springer Nature remains neutral with regard to jurisdictional claims in published maps and institutional affiliations.

**Open Access** This article is licensed under a Creative Commons Attribution-NonCommercial-NoDerivatives 4.0 International License, which permits any non-commercial use, sharing, distribution and reproduction in any medium or format, as long as you give appropriate credit to the original author(s) and the source, provide a link to the Creative Commons licence, and indicate if you modified the licensed material. You do not have permission under this licence to share adapted material derived from this article or parts of it. The images or other third party material in this article are included in the article's Creative Commons licence, unless indicated otherwise in a credit line to the material. If material is not included in the article's Creative Commons licence and your intended use is not permitted by statutory regulation or exceeds the permitted use, you will need to obtain permission directly from the copyright holder. To view a copy of this licence, visit <http://creativecommons.org/licenses/by-nc-nd/4.0/>.

© The Author(s) 2026